Biomedical Optics EXPRESS

# Broadband ultraviolet-visible optical property measurement in layered turbid media

**Quanzeng Wang,[1,*] Du Le,[2] Jessica Ramella-Roman,[2] and Joshua Pfefer[1]**

[1]*Center for Devices and Radiological Health, Food and Drug Administration, Silver Spring, MD 20993, USA*
[2]*Department of Biomedical Engineering, Catholic University of America, Washington, DC 20064, USA*
**quanzeng.wang@fda.hhs.gov*

**Abstract:** The ability to accurately measure layered biological tissue optical properties (OPs) may improve understanding of spectroscopic device performance and facilitate early cancer detection. Towards these goals, we have performed theoretical and experimental evaluations of an approach for broadband measurement of absorption and reduced scattering coefficients at ultraviolet-visible wavelengths. Our technique is based on neural network (NN) inverse models trained with diffuse reflectance data from condensed Monte Carlo simulations. Experimental measurements were performed from 350 to 600 nm with a fiber-optic-based reflectance spectroscopy system. Two-layer phantoms incorporating OPs relevant to normal and dysplastic mucosal tissue and superficial layer thicknesses of 0.22 and 0.44 mm were used to assess prediction accuracy. Results showed mean OP estimation errors of 19% from the theoretical analysis and 27% from experiments. Two-step NN modeling and nonlinear spectral fitting approaches helped improve prediction accuracy. While limitations and challenges remain, the results of this study indicate that our technique can provide moderately accurate estimates of OPs in layered turbid media.



**OCIS codes:** (170.3660) Light propagation in tissues; (170.3890) Medical optics instrumentation; (170.6510) Spectroscopy, tissue diagnostics; (170.6935) Tissue characterization; (170.7050) Turbid media.

## References and links

1. A. Jemal, R. Siegel, E. Ward, Y. P. Hao, J. Q. Xu, and M. J. Thun, "Cancer statistics, 2009," CA Cancer J. Clin. **59**(4), 225–249 (2009).
2. J. A. Freeberg, J. L. Benedet, C. MacAulay, L. A. West, and M. Follen, "The performance of fluorescence and reflectance spectroscopy for the *in vivo* diagnosis of cervical neoplasia; point probe versus multispectral approaches," Gynecol. Oncol. **107**(1 Suppl 1), S248–S255 (2007).
3. P. R. Bargo, S. A. Prahl, T. T. Goodell, R. A. Sleven, G. Koval, G. Blair, and S. L. Jacques, "*In vivo* determination of optical properties of normal and tumor tissue with white light reflectance and an empirical light transport model during endoscopy," J. Biomed. Opt. **10**(3), 034018 (2005).
4. T. J. Farrell, M. S. Patterson, and B. Wilson, "A diffusion theory model of spatially resolved, steady-state diffuse reflectance for the noninvasive determination of tissue optical properties *in vivo*," Med. Phys. **19**(4), 879–888 (1992).
5. N. Rajaram, T. H. Nguyen, and J. W. Tunnell, "Lookup table-based inverse model for determining optical properties of turbid media," J. Biomed. Opt. **13**(5), 050501 (2008).
6. D. Arifler, R. A. Schwarz, S. K. Chang, and R. Richards-Kortum, "Reflectance spectroscopy for diagnosis of epithelial precancer: model-based analysis of fiber-optic probe designs to resolve spectral information from epithelium and stroma," Appl. Opt. **44**(20), 4291–4305 (2005).
7. T. J. Farrell, M. S. Patterson, and M. Essenpreis, "Influence of layered tissue architecture on estimates of tissue optical properties obtained from spatially resolved diffuse reflectometry," Appl. Opt. **37**(10), 1958–1972 (1998).
8. S. K. Chang, D. Arifler, R. Drezek, M. Follen, and R. Richards-Kortum, "Analytical model to describe fluorescence spectra of normal and preneoplastic epithelial tissue: comparison with Monte Carlo simulations and clinical measurements," J. Biomed. Opt. **9**(3), 511–522 (2004).
9. G. Alexandrakis, T. J. Farrell, and M. S. Patterson, "Accuracy of the diffusion approximation in determining the optical properties of a two-layer turbid medium," Appl. Opt. **37**(31), 7401–7409 (1998).

#164367 - $15.00 USD Received 9 Mar 2012; revised 20 Apr 2012; accepted 23 Apr 2012; published 3 May 2012

10. T.-Y. Tseng, C.-Y. Chen, Y.-S. Li, and K.-B. Sung, "Quantification of the optical properties of two-layered turbid media by simultaneously analyzing the spectral and spatial information of steady-state diffuse reflectance spectroscopy," Biomed. Opt. Express **2**(4), 901–914 (2011).
11. Y. S. Fawzi, A. B. M. Youssef, M. H. el-Batanony, and Y. M. Kadah, "Determination of the optical properties of a two-layer tissue model by detecting photons migrating at progressively increasing depths," Appl. Opt. **42**(31), 6398–6411 (2003).
12. Q. Wang, K. Shastri, and T. J. Pfefer, "Experimental and theoretical evaluation of a fiber-optic approach for optical property measurement in layered epithelial tissue," Appl. Opt. **49**(28), 5309–5320 (2010).
13. G. M. Palmer and N. Ramanujam, "Monte Carlo-based inverse model for calculating tissue optical properties. Part I: Theory and validation on synthetic phantoms," Appl. Opt. **45**(5), 1062–1071 (2006).
14. Q. Liu and N. Ramanujam, "Scaling method for fast Monte Carlo simulation of diffuse reflectance spectra from multilayered turbid media," J. Opt. Soc. Am. A **24**(4), 1011–1025 (2007).
15. Q. Wang, A. Agrawal, N. S. Wang, and T. J. Pfefer, "Condensed Monte Carlo modeling of reflectance from biological tissue with a single illumination-detection fiber," IEEE J. Sel. Top. Quantum Electron. **16**(3), 627–634 (2010).
16. D. C. Walker, B. H. Brown, A. D. Blackett, J. Tidy, and R. H. Smallwood, "A study of the morphological parameters of cervical squamous epithelium," Physiol. Meas. **24**(1), 121–135 (2003).
17. S. Lam, B. Standish, C. Baldwin, A. McWilliams, J. leRiche, A. Gazdar, A. I. Vitkin, V. Yang, N. Ikeda, and C. MacAulay, "*In vivo* optical coherence tomography imaging of preinvasive bronchial lesions," Clin. Cancer Res. **14**(7), 2006–2011 (2008).
18. R. Reif, O. A'Amar, and I. J. Bigio, "Analytical model of light reflectance for extraction of the optical properties in small volumes of turbid media," Appl. Opt. **46**(29), 7317–7328 (2007).
19. P. Di Ninni, F. Martelli, and G. Zaccanti, "The use of India ink in tissue-simulating phantoms," Opt. Express **18**(26), 26854–26865 (2010).
20. S. K. Chang, N. Marin, M. Follen, and R. Richards-Kortum, "Model-based analysis of clinical fluorescence spectroscopy for *in vivo* detection of cervical intraepithelial dysplasia," J. Biomed. Opt. **11**(2), 024008 (2006).
21. M. Nitzan, A. Babchenko, B. Khanokh, and H. Taitelbaum, "Measurement of oxygen saturation in venous blood by dynamic near infrared spectroscopy," J. Biomed. Opt. **5**(2), 155–162 (2000).
22. R. Drezek, K. Sokolov, U. Utzinger, I. Boiko, A. Malpica, M. Follen, and R. Richards-Kortum, "Understanding the contributions of NADH and collagen to cervical tissue fluorescence spectra: modeling, measurements, and implications," J. Biomed. Opt. **6**(4), 385–396 (2001).
23. Q. Liu, C. F. Zhu, and N. Ramanujam, "Experimental validation of Monte Carlo modeling of fluorescence in tissues in the UV-visible spectrum," J. Biomed. Opt. **8**(2), 223–236 (2003).
24. Q. Z. Wang, H. Z. Yang, A. Agrawal, N. S. Wang, and T. J. Pfefer, "Measurement of internal tissue optical properties at ultraviolet and visible wavelengths: Development and implementation of a fiberoptic-based system," Opt. Express **16**(12), 8685–8703 (2008).
25. T. H. Pham, T. Spott, L. O. Svaasand, and B. J. Tromberg, "Quantifying the properties of two-layer turbid media with frequency-domain diffuse reflectance," Appl. Opt. **39**(25), 4733–4745 (2000).
26. J. C. Ramella-Roman and J. M. Hidler, "The impact of autonomic dysreflexia on blood flow and skin response in individuals with spinal cord injury," Adv. Opt. Technol. **2008**, 797214 (2008).
27. M. Kraft, K. Lüerßen, H. Lubatschowski, J. Woenckhaus, S. Schöberlein, H. Glanz, and C. Arens, "Schleimhautveränderungen im Kehlkopf: Prädiktionswert neuerer bildgebender Verfahren für eine histologische Diagnose [Mucosal lesions in the larynx: predictive value of new imaging modalities for a histological diagnosis]," HNO **56**(6), 609–613 (2008).
28. C. Arens, H. Glanz, J. Wönckhaus, K. Hersemeyer, and M. Kraft, "Histologic assessment of epithelial thickness in early laryngeal cancer or precursor lesions and its impact on endoscopic imaging," Eur. Arch. Otorhinolaryngol. **264**(6), 645–649 (2007).
29. P. R. F. Bonan, E. Kaminagakura, F. R. Pires, P. A. Vargas, and O. P. de Almeida, "Histomorphometry and immunohistochemical features of grade I (WHO) oral radiomucositis," Oral Dis. **13**(2), 170–176 (2007).
30. Q. Liu and N. Ramanujam, "Sequential estimation of optical properties of a two-layered epithelial tissue model from depth-resolved ultraviolet-visible diffuse reflectance spectra," Appl. Opt. **45**(19), 4776–4790 (2006).
31. J. E. Bender, K. Vishwanath, L. K. Moore, J. Q. Brown, V. Chang, G. M. Palmer, and N. Ramanujam, "A robust Monte Carlo model for the extraction of biological absorption and scattering *in vivo*," IEEE Trans. Biomed. Eng. **56**(4), 960–968 (2009).

## 1. Introduction

Cancers arising in mucosal tissue are responsible for approximately 200,000 deaths annually [1], and thus represent a major public health concern. Clinical studies have indicated that significant improvements in detection of early stage mucosal neoplasia may be possible with optical approaches based on ultraviolet-visible (UV-Vis) spectroscopy and imaging [2]. In order to develop numerical models that realistically describe and predict spectroscopic device performance, critical data on fundamental tissue optical properties (OPs) are needed. Furthermore, advances in OP measurement may lead to a more quantitative, reliable approach

#164367 - $15.00 USD Received 9 Mar 2012; revised 20 Apr 2012; accepted 23 Apr 2012; published 3 May 2012

for detecting subtle neoplasia biomarkers, such as changes in cellular microstructure that alter scattering properties. However, there are currently no well-established approaches for performing such measurements *in vivo*.

Most OP studies in the broadband UV-Vis range assume that tissues are homogenous. Bargo *et al.* used a dual-fiber probe to deliver white light and measure reflectance from tissue using a diode array spectrophotometer [3]. This study used the diffusion approximation [4] to simulate light transport from the illumination fiber to the detection fiber. Rajaram *et al.* [5] performed UV-Vis OP measurements in homogenous phantoms with a fiber-optic probe based on a look-up table generated from experimental measurement of phantoms. This study involved determination of hemoglobin (Hb)-based phantom OPs over a wide range of absorption ($\mu_a$, 0-53.3 $cm^{-1}$) and reduced scattering ($\mu_s'$, 2.2-71 $cm^{-1}$) coefficients.

In recent years there has been increasing interest in OP measurement in layered tissue, since most mucosal tissues (e.g., cervix, esophagus and colon) consist of distinct layers. Normal cervical tissue, for example, comprises a squamous epithelial layer 0.2-0.5mm thick above a stromal layer that is sufficiently thick as to be considered semi-infinite for UV-Vis spectroscopy [6,7]. *In vitro* studies have indicated that layer-specific changes in the fundamental OPs of mucosal tissues—absorption and scattering coefficients—occur during carcinogenesis [8]. Farrell *et al.* [7] and Alexandrakis *et al.* [9] performed theoretical studies relevant to near-infrared spectroscopy of two-layer tissues in which top-layer thickness (D) ranged from 1 to 2.5 mm. A more recent study of two-layer turbid media by Tseng *et al.* [10] involved simultaneous analysis of spectral and spatial reflectance data. A nonlinear curve fitting method was used to estimate OPs, however, no layered phantom or tissue was measured. Fawzi *et al.* [11] determined the OPs of a two-layer phantom at 660 nm by deducing the top- and bottom- layer OPs in two steps. The phantom consisted of $Al_2O_3$ as scatterer and dyes as absorbers. The method is useful for OP measurement only when D is greater than 5 mm. In our previous study we developed experimental and analytical approaches for determining OPs in two-layer turbid media over a wide range of $\mu_a$ (1.0-22.5 $cm^{-1}$) and $\mu_s'$ (5.0-42.5 $cm^{-1}$) at three UV-Vis wavelengths (375, 445, and 543nm) using a fiber-optic-based reflectance system [12]. In order to generate a thorough description of tissue OPs relevant to optical spectroscopy, however, broadband UV-Vis measurements are needed.

The intent of this study was to develop a simple and accurate fiber-optic approach for determination of broadband OPs of layered mucosal tissue in the UV-Vis, enabling discrimination of normal and dysplastic mucosa. We developed neural network (NN) inverse models and a fitting algorithm for estimating OPs in two-layer turbid media over the 350-600 nm range. The accuracy of our approach was initially evaluated using simulated reflectance data with and without added noise. We then performed an experimental assessment by measuring two-layer phantoms simulating normal and neoplastic mucosal tissues.

## 2. Methods

A multi-stage OP estimation approach was developed, including inverse NN models trained with data from two-layer Monte Carlo (MC) simulations and a nonlinear spectral fitting algorithm. Evaluation of this technique was performed through theoretical analyses of simulated reflectance data as well as experimental broadband measurements of tissue phantoms with a UV-Vis fiber-optic reflectance spectroscopy system.

### *2.1. Model development*

#### 2.1.1. Condensed two-layer MC model

A condensed two-layer MC model [12–15] was used to generate an extensive set of OP-reflectance data. The model began with a baseline MC simulation. The homogeneous medium used for the baseline simulation in the condensed MC modeling was assigned the following OPs: $\mu_a$ = 1 $cm^{-1}$, $\mu_s$ = 100 $cm^{-1}$, and $g$ = 0.9 ($\mu_s'$ = 10 $cm^{-1}$). The index of refraction ($n$) of the

#164367 - $15.00 USD Received 9 Mar 2012; revised 20 Apr 2012; accepted 23 Apr 2012; published 3 May 2012

fibers was 1.46 and $n$ = 1.34 for the tissue. In the baseline simulation 6,000,000 photons were launched in uniform spatial distribution over the fiber face and angular distribution specified by the numerical aperture (NA) of 0.22. Convolution and scaling equations were then employed to generate reflectance data based on over 20,000 sets of OPs of two-layer tissues distributed at regular intervals over the following ranges: 0.01 –25 $cm^{-1}$ for $\mu_a$ and 1-50 $cm^{-1}$ for $\mu_s'$. The probe geometry was based on the experimental fiber-optic probe design and our primary probe-geometry optimization results. It consisted of seven linearly arranged fibers, one for illumination and 6 for detection (Fig. 1) with illumination-collection distances of 0.25, 0.5, 1.0, 1.5, 2.0 and 2.25 mm (center-to-center). Each fiber had a core diameter of 0.2 mm and an NA of 0.22.

#### 2.1.2. Two-stage inverse NN modeling

MC-generated data were used to train feed-forward back-propagation NN inverse models. The NN models were designed to predict four OPs of a two-layer tissue [top-layer $\mu_a$ ($\mu_{a1}$), top-layer $\mu_s'$ ($\mu_{s1}'$), bottom-layer $\mu_a$ ($\mu_{a2}$) and bottom-layer $\mu_s'$ ($\mu_{s2}'$)] per wavelength based on spatially-resolved reflectance inputs. Due to the large parameter space and number of simulations required, each NN model was trained with data based on a specific D value. Thus, this approach assumed *a priori* knowledge of D. Two D values were studied: 0.22 and 0.44 mm. These values are within the range that occurs in normal and neoplastic cervical tissue [16], although in some epithelial tissues, superficial layer thickening may correlate with neoplasia [17]. For each D value, two NN models (NN#1 and NN#2) were developed. Each NN model had six inputs, two hidden layers of seven neurons each and an output layer of four neurons, and was developed based on simulated reflectance data ($12^4$ data sets). The six inputs were reflectance values from detection fibers of the probe (Fig. 1). In the NN models, 12 $\mu_{a1}$ values and 12 $\mu_{a2}$ values at regular intervals were used over ranges of 0.1-25 $cm^{-1}$ for NN#1 and 0.01-5 $cm^{-1}$ for NN#2, and 12 $\mu_{s1}'$ values and 12 $\mu_{s2}'$ values at regular intervals were used over a range of 1-50 $cm^{-1}$ for both NN#1 and NN#2.

The OPs of two-layer tissues were estimated in two stages. For any set of reflectance values, NN#1 was applied initially. If the predicted $\mu_{a2}$ value was below 4 $cm^{-1}$, NN#2 was used to obtain the final results. Otherwise, the OPs from NN#1 were recorded as the final results. We called this two-stage approach the "2NN" approach. On the other hand, if only NN#1 was used to get the final results for all the OP range, the one-stage approach was called "1NN" approach. By performing this process for each reflectance distribution at each wavelength, it was possible to generate OP spectra.

#### 2.1.3. Fitting algorithms

A nonlinear least squares fitting routine was used to optimize the NN-predicted OP spectra based on established spectral signatures of tissue scatterers and absorbers [18,19]. The OPs after fitting were called results from the "FIT" approach. The fitting equation for $\mu_s'$ was $\mu_s' = a \cdot \lambda^b$, where $\lambda$ is the wavelength, $a$ and $b$ are fitting coefficients [18]. Since the absorbance spectrum of the top layer is expected to be monotonically decreasing with wavelength, the following fitting equation was used: $\mu_{a1} = a \cdot \lambda^b$ [19]. Because the true values of $\mu_{a1}'$, $\mu_{s1}'$ and $\mu_{s2}'$ should decrease with wavelength, the restriction $b < 0$ was implemented.

Given the findings of prior studies [18], bottom-layer absorption was assumed to be a linear contribution of the predominant absorbers Hb and $HbO_2$. Thus, the fitting equation was $\mu_{a2} = f_1 \cdot [f_2 \cdot \varepsilon_{HbO2} + (1- f_2) \cdot \varepsilon_{Hb}]$, where $f_1$ is the total concentration of Hb, $f_2$ is the oxygen saturation, and $\varepsilon_{HbO2}$ and $\varepsilon_{Hb}$ are molar extinction coefficients of oxygenated and deoxygenated Hb. The value of $f_2$ was restricted between 70% and 100% according to the literature [20,21].

#164367 - $15.00 USD Received 9 Mar 2012; revised 20 Apr 2012; accepted 23 Apr 2012; published 3 May 2012

*2.2. Theoretical evaluation*

The inverse modeling and fitting components of our OP measurement approach were evaluated using reflectance data generated from condensed MC simulations based on hypothetical two-layered phantoms. The two cases studied used the same OP ranges based on data from *in vitro* measurements of normal layered- bronchial [8] and cervical [22] tissues, but different D values: 0.22 and 0.44 mm. The bottom-layer thickness of each phantom was 2 cm which was considered as semi-infinite. OP values were based on the hypothetical phantoms in which the top- and bottom-layer absorbers were India ink with a volume concentration of 0.05% and Hb with the concentration of 1.8 mg/mL respectively. Scattering was based on microsphere (1 μm diameter, polystyrene) concentrations in top and bottom layers of 0.2% and 0.7% (by weight), respectively. The true, or target OPs (TAR) of these imaginary phantoms were calculated by applying Beer's law from the actual absorbance of pure solute absorbers measured with a spectrophotometer for $\mu_a$ and Mie theory for $\mu_s'$. The OP results from the approach were compared with the TAR values for situations without noise and with 5% uniform random noise added to the reflectance.

*2.3. Experimental evaluation*

2.3.1. Broadband reflectance spectroscopy system

The reflectance spectroscopy system (Fig. 1) incorporated a 35 Watt xenon lamp (HPX-2000, Ocean Optics, Dunedin, FL), a custom designed fiber-optic probe, a spectrograph with cooled imaging CCD (Insight 400, Princeton Instruments, Trenton, NJ) and a laptop with MATLAB® (Mathworks, Natick MA) running customized routines. The probe geometry was the same as described in Section 2.1.1. The legs of the probe were connected to in-line neutral density (ND) filters to attenuate short separation distance fibers and thus enable simultaneous measurements of all fibers at the CCD while maximizing the useable dynamic range.

The system was calibrated before each measurement. Reflectance ($R$) from a detection fiber is the fraction of incident light from the illumination fiber that is collected by this detection fiber ($I$). Its value at each wavelength is proportional to $I$ over intensity collected from a Spectralon® target ($I_0$) by a calibration factor ($k$) as shown in Eq. (1). Since OPs of a tissue are a function of wavelength (λ), $R$, $I$ and $I_0$ are also functions of λ. The introduction of $I_0$ can reduce the error from the power variations between operations.

$$R(\lambda) = k(\lambda)\frac{I(\lambda)}{I_0(\lambda)} \tag{1}$$

The value of $k(\lambda)$ for each detection fiber was obtained through calibration. During calibration, a series of five single-layer tissue-simulating phantoms were created from deionized water, 1 μm diameter polystyrene microspheres (Polybead® Microspheres, Polysciences, Inc.) and nigrosin (Sigma N4754). The OP ranges of these phantoms were 2.14-10.5 $cm^{-1}$ for $\mu_a$ and 4-32 $cm^{-1}$ for $\mu_s'$. For each phantom, theoretical $R(\lambda)$ from each detection fiber was calculated with the condensed MC algorithm based on the theoretical $\mu_a(\lambda)$ and $\mu_s'(\lambda)$ of phantoms according to Beer's law and Mie theory. $I(\lambda)$ was measured from contact measurement of phantoms whereas $I_0(\lambda)$ was measured from a Spectralon® target at a distance of 1 cm. For each fiber and at each wavelength, a graph of $R(\lambda)$ versus $I(\lambda)/I0(\lambda)$ was constructed based on the data from all the phantoms and used to determine a linear best fit. The slope of this line was $k(\lambda)$ which should remain constant for different tissues. Once $k(\lambda)$ for each detection fiber was obtained, $R(\lambda)$ of a phantom was calculated according to Eq. (1) and used to estimate OPs with our two-stage NN-based inverse model.

2.3.2. Layered phantom measurements

Experimental measurements were performed on four two-layer, tissue-simulating phantoms. Two of these phantoms simulated normal epithelial tissues (with D = 0.22 and 0.44 mm) and

#164367 - $15.00 USD Received 9 Mar 2012; revised 20 Apr 2012; accepted 23 Apr 2012; published 3 May 2012

two simulated dysplastic epithelial tissues with the same D values. The OP ranges of these phantoms were based on *in vitro* data for bronchial [8] and cervical [22] tissues from the literature. The differences between normal and dysplastic phantoms account for molecular and structural changes that occur in individual mucosal tissue layers with neoplastic progression, including increased scattering from epithelial cells, decreased scattering from collagen fibers in the stroma, and increased absorption in the stroma due to angiogenesis [6].

Phantoms were constructed with deionized water, agarose (Type VII, Sigma A-9045), Hb (Hb A0, ferrous stabilized human, Sigma H0267), black India ink (Waterproof, Higgins) and 1.0 μm diameter polystyrene microspheres (Polybead® Microspheres, Polysciences, Inc.). Type VII agarose was chosen for its low gelling temperature and easy construction of layered phantoms. Microspheres and Hb were chosen for their optical similarity to tissue scatterers and chromophores in the UV-Vis spectral range. Microspheres of 1 μm diameter have commonly been used to simulate the cellular and structural protein scatters in tissue [23]. The final concentration of agarose in phantom was 1%. In order to evaluate the potential for phantom fluorescence to affect OP estimates, we performed fiber-optic measurements of a microsphere-agarose phantom using laser sources at 375, 405, 445 and 543 nm and the aforementioned spectrograph and camera (Fig. 1). The signal levels detected by each fiber in spectral regions between the laser lines and 600 nm were more than 4 orders of magnitude less than that detected at the illumination wavelength. Furthermore, given the extremely low quantum yield of tissue fluorophores, it is unlikely that diffuse reflectance would be significantly affected by endogenous fluorescence. According to the target OP values of each layer, the concentrations of absorbers (Hb and ink) were calculated by applying Beer's law for absorbance of pure solute absorbers measured with a spectrophotometer (UV-3100PC, Shimadzu Inc., Columbia, MD) and that of microspheres were calculated with Mie theory. The structure and composition of the two normal epithelial tissue phantoms were the same as that of the hypothetical phantoms described in Section 2.2. Compared with the phantoms simulating normal tissues, the two phantoms simulating dysplastic tissues had the following differences: (1) top-layer microsphere concentration was increased from 0.2% to 0.5% in order to simulate increased cell density, (2) bottom Hb was increased from 1.8 to 2.7 mg/mL to simulate the increased blood content, and (3) bottom-layer microsphere concentration was decreased from 0.7% to 0.5% to simulate degraded collagen fibers.

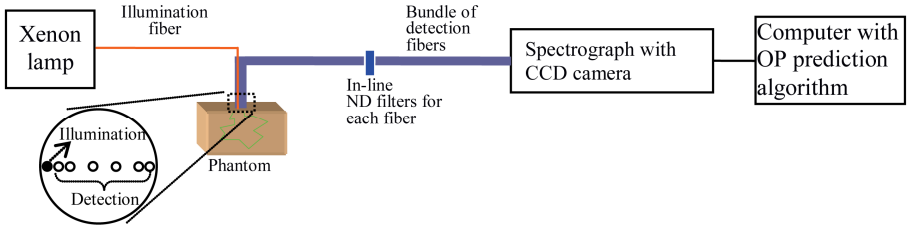


Fig. 1. Diagram of diffuse reflectance spectroscopy system for OP measurement.

To construct a phantom, the agarose-water mixture was heated at 65°C until the agarose dissolved. Measurements showed that the agarose gel was transparent in 350-600 nm. Another water-Hb-microsphere mixture was warmed at 40 °C (overheating of the mixture may change the absorption spectra of Hb) for 2 minutes and combined with the water-agarose solution. The final mixture was then transferred into a small cylindrical container with diameter and thickness of 2 cm to achieve a bottom layer that was essentially semi-infinite. By molding the phantom mixture between two microscope slides using cover slips (0.22 mm thickness) as spacers, it was possible to achieve top phantom layers that were 0.22 and 0.44 mm thick. No membrane was used between these two layers since experiments showed that a membrane would affect the reflectance signal if the top layer was thinner than 0.66 mm. In each case, three two-layered phantoms with same OPs were created and the mean estimated OPs were

#164367 - $15.00 USD Received 9 Mar 2012; revised 20 Apr 2012; accepted 23 Apr 2012; published 3 May 2012

determined. Mean standard deviation of all cases was 1.9 $cm^{-1}$. To perform a measurement, the fiber-optic probe was placed gently on a phantom such that the tip was flush with the phantom surface. By measuring the layered phantom OPs and comparing results with the target values it was possible to determine measurement accuracy.

## 3. Results

### *3.1. Theoretical evaluation of the OP measurement approach*

Figure 2 shows a comparison of four curves for each OP parameter and D value considering noise-free reflectance of the hypothetical phantoms: (1) the TAR values from Beer's law and Mie theory; (2) the values from the 1NN approach; (3) the values from the 2NN approach; and (4) the fitted values based on 2NN (FIT). With the TAR values as reference, Table 1 quantitatively summarizes the absolute and percentage mean errors of 1NN, 2NN and FIT approaches. The results in Fig. 2 indicate that fitting significantly improved the agreement between predicted and target OPs by removing noise and irregular features seen in predicted $\mu_{a1}$, $\mu_{s1}'$, and $\mu_{s2}'$ values at 380–440 nm. Quantitatively, the 2NN approach reduced OP prediction error ($cm^{-1}$) of the 1NN approach by 39% when D was 0.22 mm and 44% when D was 0.44 mm. Corresponding values for the FIT approach were 53% and 61%. In general, both the 2NN and the FIT approaches significantly reduced the 1NN predicted errors of all the OPs for both thicknesses. Fitting produced further reduction in 2NN-predicted errors by 22% and 28% when D was 0.22 and 0.44 mm, respectively. The fitting algorithm was most effective for $\mu_{s1}'$ when D was 0.44 mm, with the error of 0.46 $cm^{-1}$ (or 6%). Mean error results presented in Table 1 indicate moderate levels of accuracy across OPs and cases, although, on average $\mu_s'$ estimation was more accurate than $\mu_a$ (9% vs. 29% error, respectively).

Figure 3 provides a composite assessment of all predicted OP values in Fig. 2. The $\mu_a$ results [Fig. 3(a)] include data for $\mu_{a1}$ and $\mu_{a2}$ and indicate good agreement across more than two orders of magnitude variation. Predictions of $\mu_s'$, including $\mu_{s1}'$ and $\mu_{s2}'$, also show good agreement, although the range of $\mu_s'$ values is much more limited [Fig. 3(b)]. Linear fits to data in Fig. 3(a) and Fig. 3(b) have $R^2$ values of 0.89 and 0.91, respectively. In both cases, a significant component of the error was due to OPs of thin superficial layers; by removing data for D = 0.22 mm, $R^2$ values improved to 0.95 and 0.94.

Nonlinear spectral fitting was especially valuable if there was noise in the reflectance signal. As an example, Fig. 4 shows the bottom layer OPs for D = 0.22 mm based on the 2NN and FIT approaches when 5% noise was added to the reflectance. This figure illustrates the degree to which the fitting approach smoothed and improved 2NN predicted OP spectra. A summary of mean errors for all OPs and both D values in the 5% added noise case are shown in Table 2. Again, when D = 0.44 mm, the FIT approach achieved the most accurate results for $\mu_{s1}'$ (4%) which otherwise had the largest error (77%) based on 2NN estimates. Comparing Table 1 and Table 2, noise significantly increased prediction errors of the 2NN approach, by 84% when D = 0.22 mm and by 44% when D = 0.44 mm. However, these values were 48% and 0% for the FIT approach, indicating a significant reduction in the effect of noise on prediction accuracy.

The prediction of OPs with the FIT approach was strongly related to D (Fig. 5). As D increased from 0.22 mm to 0.44 mm, prediction error of top-layer OPs decreased by 42% while that of bottom layer OPs increased by 40% in noise-free case. These trends are in agreement with expected variations in accuracy based on prior studies of layered turbid media [7,12]. In both noise-free and noise-added cases the predicted top-layer OPs were more accurate when D was 0.44 mm than when D was 0.22 mm. This was likely due to the fact that the fraction of detected photon path lengths spent in the superficial layer (and thus sensitivity to that layer) was directly related to D. On the other hand, the prediction of bottom layer OPs was more accurate when D was 0.22 mm than when D was 0.44 mm for the noise-free case.

#164367 - $15.00 USD Received 9 Mar 2012; revised 20 Apr 2012; accepted 23 Apr 2012; published 3 May 2012

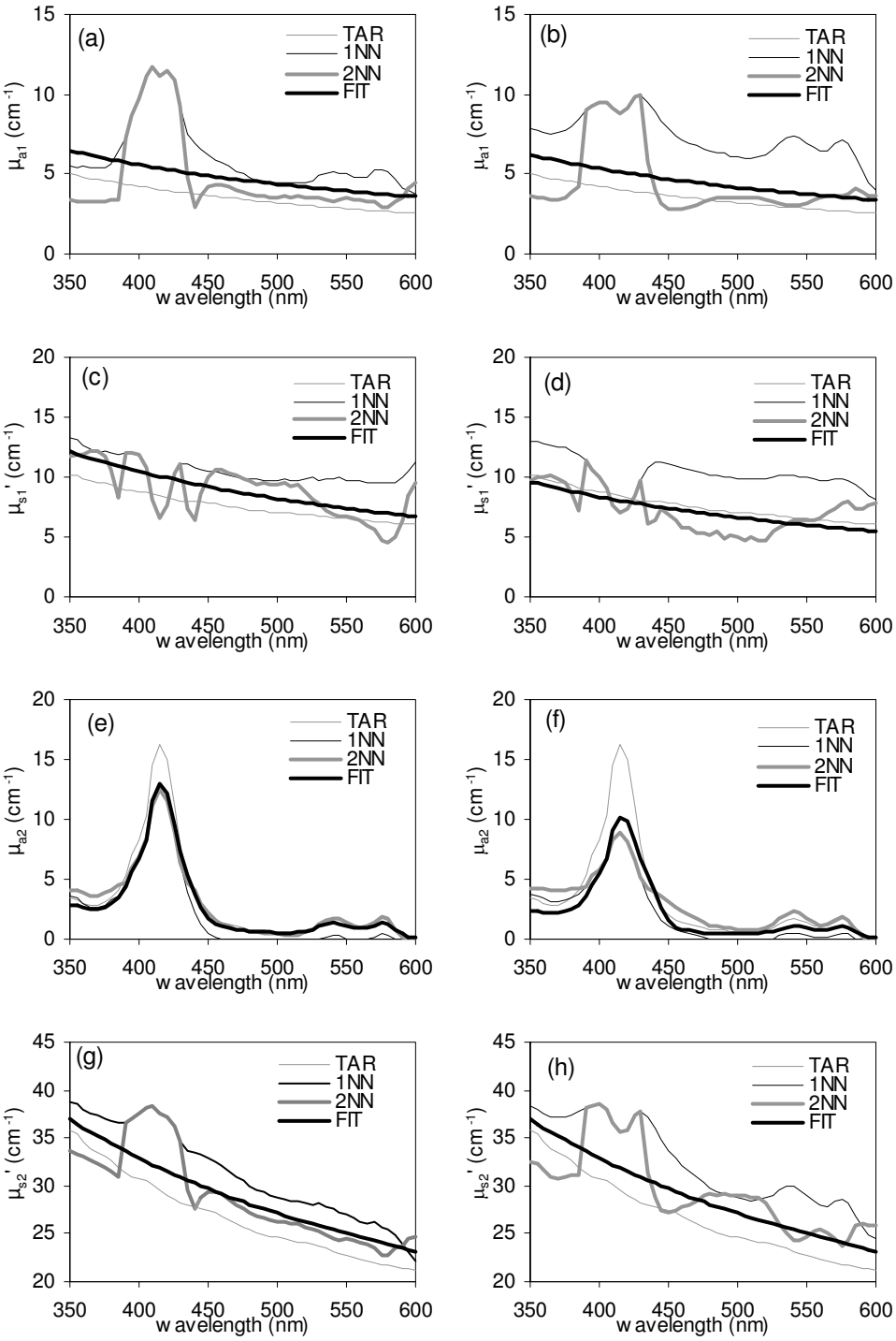


Fig. 2. Theoretical evaluation of OP prediction accuracy for D = 0. 22 mm (a, c, e, g) and D = 0.44 mm (b, d, f, h). TAR: target values from Beer's law and Mie theory; 1NN: values from NN#1; 2NN: values from NN#1 and NN#2; FIT: fitted values based on 2NN.

#164367 - $15.00 USD Received 9 Mar 2012; revised 20 Apr 2012; accepted 23 Apr 2012; published 3 May 2012

**Table 1. Mean OP Estimation Errors**

| | Error ($cm^{-1}$) | | | | | | Error (percentage) | | | | | |
|---|---|---|---|---|---|---|---|---|---|---|---|---|
| | D = 0.22 mm | | | D = 0.44 mm | | | D = 0.22 mm | | | D = 0.44 mm | | |
| | 1NN | 2NN | FIT | 1NN | 2NN | FIT | 1NN | 2NN | FIT | 1NN | 2NN | FIT |
| $\mu_{a1}$ | 2.5 | 1.7 | 1.2 | 3.8 | 1.5 | 1.0 | 72% | 44% | 35% | 111% | 39% | 29% |
| $\mu_{s1}'$ | 2.9 | 1.8 | 1.3 | 2.8 | 1.3 | 0.5 | 39% | 23% | 16% | 37% | 17% | 6% |
| $\mu_{a2}$ | 1.1 | 0.6 | 0.5 | 1.4 | 1.1 | 1.0 | 65% | 22% | 16% | 61% | 35% | 29% |
| $\mu_{s2}'$ | 4.7 | 2.7 | 2.2 | 5.6 | 3.6 | 2.8 | 18% | 10% | 8% | 21% | 14% | 11% |
| Average | 2.8 | 1.7 | 1.3 | 3.4 | 1.9 | 1.3 | 49% | 25% | 19% | 58% | 26% | 19% |

**Table 2. Mean OP Estimation Errors with 5% noise**

| | Errors ($cm^{-1}$) | | | | Errors (percentage) | | | |
|---|---|---|---|---|---|---|---|---|
| | D = 0.22mm | | D = 0.44mm | | D = 0.22mm | | D = 0.44mm | |
| | 2NN | FIT | 2NN | FIT | 2NN | FIT | 2NN | FIT |
| $\mu_{a1}$ | 2.6 | 1.3 | 1.9 | 0.7 | 73% | 34% | 58% | 20% |
| $\mu_{s1}'$ | 5.8 | 1.5 | 5.8 | 0.3 | 78% | 20% | 77% | 4% |
| $\mu_{a2}$ | 0.8 | 1.2 | 0.6 | 0.9 | 30% | 39% | 18% | 29% |
| $\mu_{s2}'$ | 3.3 | 3.8 | 2.5 | 3.4 | 13% | 15% | 10% | 14% |
| Average | 3.1 | 1.9 | 2.7 | 1.3 | 48% | 27% | 41% | 17% |

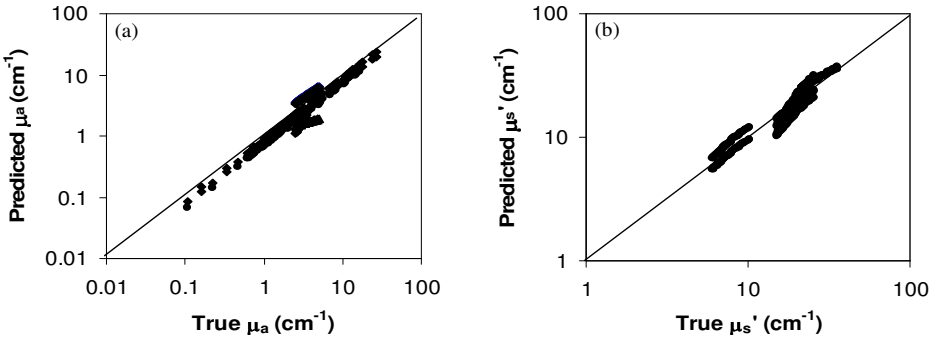


Fig. 3. Theoretical estimates of OP prediction accuracy based on data from Fig. 2.

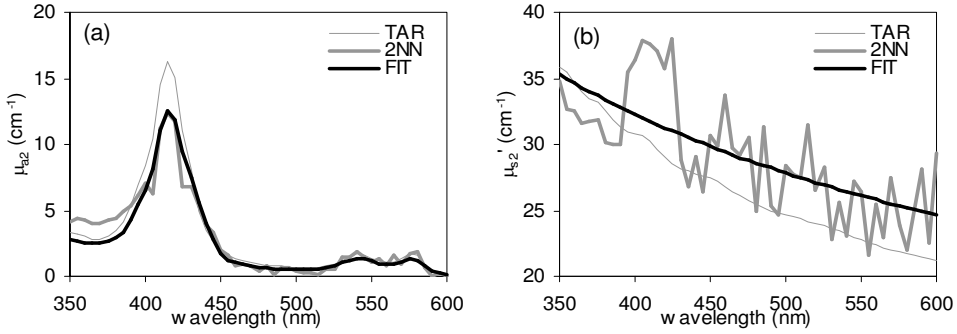


Fig. 4. Theoretical evaluation of 2NN and FIT approaches based on reflectance data with added noise (D = 0.22 mm).

#164367 - $15.00 USD Received 9 Mar 2012; revised 20 Apr 2012; accepted 23 Apr 2012; published 3 May 2012

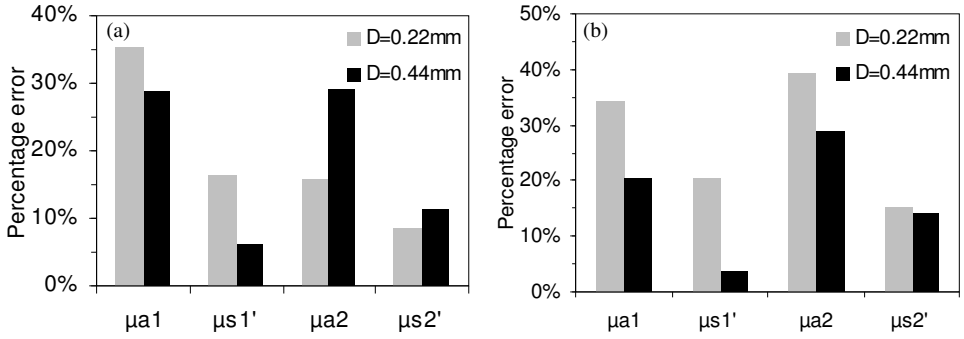


Fig. 5. Summary of the theoretical accuracy of our OP predication method using (a) noise-free and (b) noise-added reflectance data.

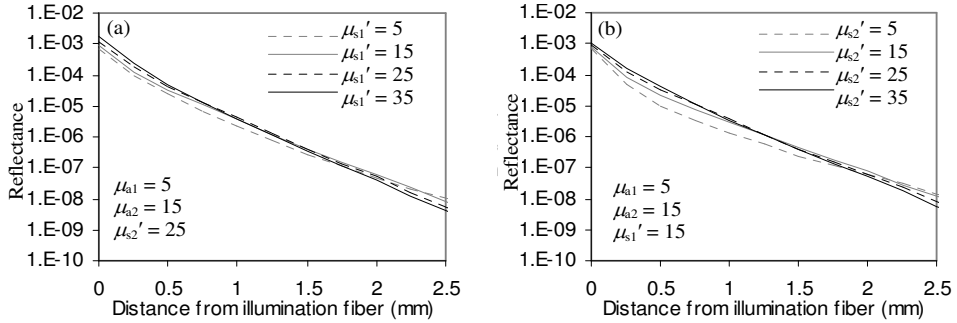


Fig. 6. Simulation results showing reflectance as function of distance from center of illumination fiber and OPs when D = 0.44 mm: numbers in the legends have units of $cm^{-1}$. (a) Change in $\mu_{s1}'$ and (b) change in $\mu_{s2}'$

While the conclusions for the noise-free case did not hold for the bottom layer OPs of the noise-added case, they were true for the top-layer OPs with the $\mu_{s1}'$ prediction having the smallest error (4%) when D was 0.44 mm.

The erroneous spectral shape of predicted $\mu_{a1}$, $\mu_{s1}'$ and $\mu_{s2}'$ spectra with the 2NN approach (Fig. 2 and Fig. 4) in the 380-450 nm range was likely due to crosstalk—when one OP parameter influences the prediction accuracy of other OPs [7]. Since we did not see crosstalk when using single layered model [24], it is likely that this effect increases with number of output parameters, along with OP estimation error [25]. In addition, at high $\mu_{a2}$, simulated reflectance values were similar regardless of the other OP values as illustrated in Fig. 6. As a result, prediction accuracy was low at high values of $\mu_{a2}$. A similar case occurs at high $\mu_{s2}'$.

### *3.2. Experimental measurement of two-layer-phantom OPs*

The predicted OPs from phantoms representing normal and dysplastic epithelial tissues are shown in Fig. 7 and Fig. 8. These figures compare experimental OP estimates with true values from the top layer [Figs. 7(a), 7(b), Figs. 8(a), 8(b)] and bottom layer [Figs. 7(c), 7(d), Figs. 8(c), 8(d)] for normal (Fig. 7) and dysplastic (Fig. 8) tissues. They show generally good agreement between predicted and true phantom OP spectra. The $\mu_{a2}$ predictions were relatively accurate as a whole, although at certain longer wavelengths in the normal case where $\mu_{a2}$ was particularly low, errors exceeded 40%.

Table 3 summarizes mean prediction errors from the aforementioned figures. This data indicates that prediction of $\mu_{s1}'$ had the greatest error when D was 0.22 mm. The reason was that the top layer was so thin and minimally attenuating that it had a minor impact on light propagation and thus detected reflectance carried little information of this layer. On the other

#164367 - $15.00 USD Received 9 Mar 2012; revised 20 Apr 2012; accepted 23 Apr 2012; published 3 May 2012

hand, when D = 0.44 mm mean prediction errors for $\mu_s'$ cases were all less than 18%. In general, Table 3 shows higher mean errors than the theoretical results (Table 1), due to

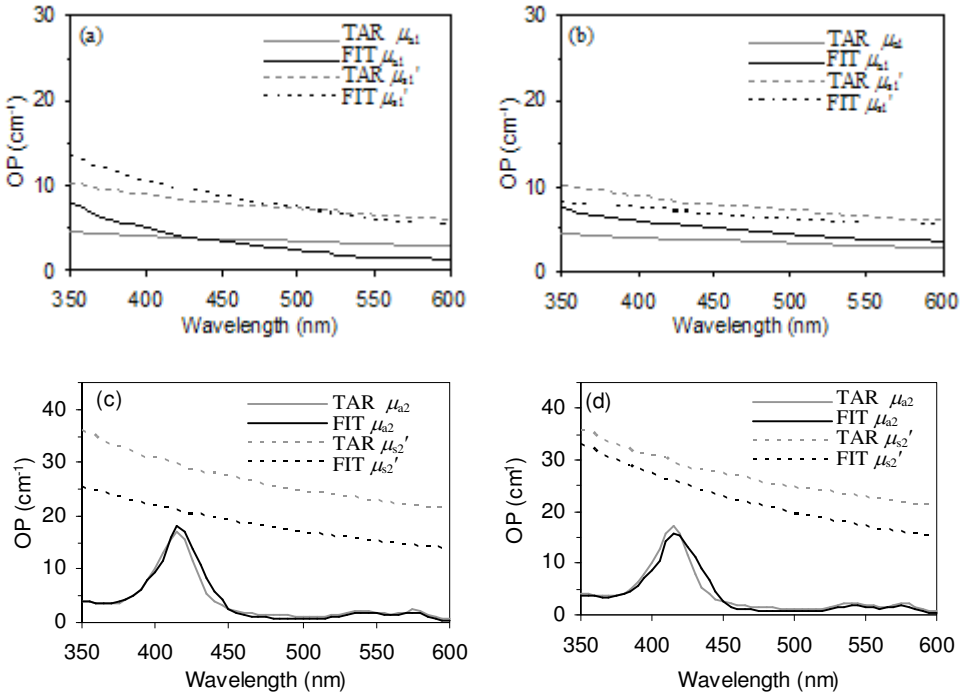


Fig. 7. Experimental evaluation of OP estimates (FIT) as compared to target/true (TAR) values for phantoms representing normal mucosal tissue [D = 0.22mm: (a), (c); D = 0.44mm: (b), (d)].

experimental error. This includes detector noise, particularly for large separation distance fibers and high attenuation conditions, and variations in true phantom OPs and thickness.

While the variations in accuracy with D shown in Table 3, are not strong and monotonic as in our prior study [12], the impact of top-layer thickness on accuracy is evident to some degree. Three of the four highest error entries in this table represent top-layer OPs in phantoms with thin superficial layers (D = 0.22 mm). As D was increased to 0.44 mm, there was strong improvement in accuracy of top-layer OPs for the dysplastic phantom, although no corresponding trend is seen for the normal phantoms. The influence of D on OP estimation accuracy is due to mean relative pathlength in each layer for detected photons, and thus relative sensitivity to each layer, which is related to fiber-optic probe design. The lessening of this effect in the experimental results may be due to a number of factors, including noise in the reflectance data, the low attenuation in the superficial layer and crosstalk effects.

Because of the crosstalk, large errors in top-layer OPs were produced during two-layer estimates. These results can be compared to results for a single-layer tissue, and thus prediction of a single scattering and absorption coefficient for each sample. Figure 9 shows experimental OP measurements for single-layer phantoms. This involved use of an algorithm similar to FIT, and a NN model with two output values instead of four. The target OPs in Figs. 9(a), 9(b) were the same as those of top- [Fig. 7(a)] and bottom- [Fig. 7(c)] layer OPs of the phantom representing normal tissue. The mean errors in both graphs of Fig. 9 were 4%, which can be compared with mean two-layer errors of 23% in Fig. 7(a) and 26% in Fig. 7(c).

#164367 - $15.00 USD Received 9 Mar 2012; revised 20 Apr 2012; accepted 23 Apr 2012; published 3 May 2012

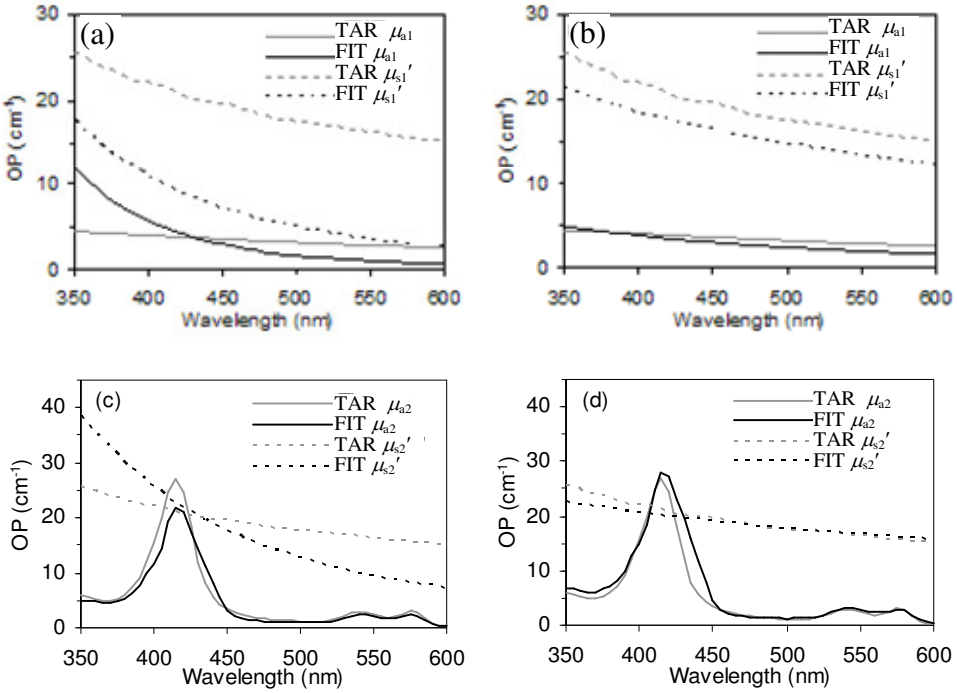


Fig. 8. Experimental evaluation of OP estimates based on phantoms representing dysplastic mucosal tissue [D = 0.22mm: (a), (c); D = 0.44mm: (b), (d)].

**Table 3. Mean OP prediction errors from phantoms**

| | Errors (cm$^{-1}$) | | | | Errors (percentage) | | | |
|---|---|---|---|---|---|---|---|---|
| Phantoms | Normal | | Dysplastic | | Normal | | Dysplastic | |
| D (mm) | 0.22 | 0.44 | 0.22 | 0.44 | 0.22 | 0.44 | 0.22 | 0.44 |
| $\mu_{a1}$ | 1.1 | 1.5 | 2.0 | 0.6 | 34% | 42% | 58% | 19% |
| $\mu_{s1}'$ | 1.0 | 1.2 | 11.8 | 3.1 | 12% | 15% | 64% | 16% |
| $\mu_{a2}$ | 0.5 | 0.7 | 1.0 | 1.0 | 21% | 27% | 18% | 18% |
| $\mu_{s2}'$ | 8.2 | 4.6 | 5.3 | 0.8 | 31% | 18% | 29% | 4% |
| Average | 2.7 | 2.0 | 5.0 | 1.3 | 25% | 26% | 42% | 14% |

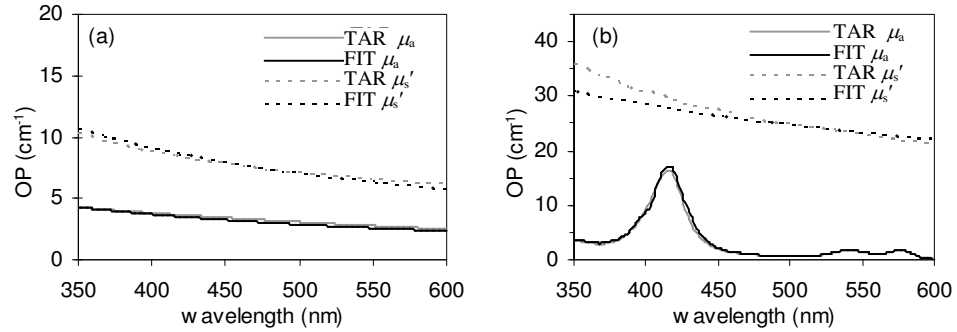


Fig. 9. OP predictions based on experimental measurements of single-layer phantoms representing the (a) top and (b) bottom layers of normal tissue.

#164367 - $15.00 USD Received 9 Mar 2012; revised 20 Apr 2012; accepted 23 Apr 2012; published 3 May 2012

## 4. Discussion

Our prior study with UV-Vis lasers [12] shows that there is a strong relationship between D and prediction accuracy of OPs. As D increases from 0.22 mm to 0.44 mm, the prediction of top-layer OPs improves significantly while that of bottom layer OPs gets worse. While the theoretical study of noise-free cases showed the same trend, it was not completely true for the theoretical study of noise-added cases and the experimental study. On average, estimated mean errors in the experimental study were 1.6 $cm^{-1}$ (46%) for $\mu_{a1}$, 6.4 $cm^{-1}$ (38%) for $\mu_{s1}'$, 0.8 $cm^{-1}$ (20%) for $\mu_{a2}$ and 6.8 $cm^{-1}$ (30%) for $\mu_{s2}'$ when D = 0.22 mm. When D = 0.44 mm, these numbers were 1.0 $cm^{-1}$ (31%), 2.1 $cm^{-1}$ (16%), 0.9 $cm^{-1}$ (22%) and 2.7 $cm^{-1}$ (11%). On average, both the top and bottom OPs were more accurate when D was 0.44 mm than when D was 0.22 mm. This could be explained by the fact that the prediction accuracy of both layers is linked by the use of a single NN model that simultaneously estimates all four values, thus an erroneous prediction of OPs in one layer may affect predictions for the other.

As seen in both theoretical evaluation and experimental measurements, $\mu_{a2}$ had a strong impact on the prediction accuracy of other OPs, especially near Hb absorption peaks at 380-440 nm. The influence of Hb absorption on OPs was studied by Bargo *et al.* [3]. As shown in their results, the OP analysis using fiber-based reflectance allows the crosstalk between absorption and scattering at highly absorptive wavelengths. In our experimental results, the mean errors of bottom layer OPs did not change significantly when D increased from 0.22 to 0.44 mm. These results implied that, compared with the effect of D, noise and crosstalk effect contributed a larger impact on the prediction of OPs when D was small. Crosstalk in prediction of layered tissue OPs has been also noted in prior studies [7,12]. However, these features were not noted at all wavelengths, tended to be localized spectrally and had a relatively minor impact on overall prediction accuracy.

The benefit of using spectral fitting for OP data was significant, likely due in part to the averaging of errors across the measured spectrum. Overall, fitting improved the error range of experimental OP prediction from 39 to 67% to 21-38%. Analysis of unfitted predictions generated by the NN model was also useful in identifying sources of error. One key feature in some of these predictions was a significant impact of the Hb Soret absorption band near 415 nm on prediction of $\mu_{a1}$, $\mu_{s1}'$, and $\mu_{s2}'$. The similar fitting approach was used by Bargo *et al.* [3], Reif *et al.* [18] and Ramella-Roman and Hidler [26] to calculate total reflectance. However, the comparison between original OPs and fitted OPs was not available in these studies.

Top-layer thickness is a key factor in determination of layered tissue OPs and may be significant for neoplasia detection. Studies on epithelial thickness in early laryngeal cancer show that the vocal fold mucosa thickens progressively with dysplasia, while additional inflammation did not have any significant influence on the total epithelial thickness [27,28]. A prior study indicated that epithelial thickness is decreased in oral mucositis and inflammatory components [29]. Investigation of bronchial epithelium by Lam *et al.* shows that mild, moderate and severe dysplasia are significantly thicker than metaplasia (P = 0.002) [17]. On the other hand, Walker *et al.* show that the thickness of cervical squamous epithelium is not correlated with tissue pathology [16]. While there is no general consensus about the correlation between epithelial thickness and tissue pathology for epithelial tissues, a relationship may exist for specific tissue types and/or conditions. Ideally, a NN model could be developed which accounted for the four OP values as well as D, however, this would be highly challenging due to the quantity of training data required and the likely increase in uncertainty of predicted values. In a prior study, results indicated that the accuracy of OP and D predictions degrade strongly with number of unknowns [25]. For a three-variable fit, the accuracy levels of 19% for D, 21% for $\mu_a$ and 6% for $\mu_s'$. No results were presented for four-variable fits and prediction of five unknowns produced errors "typically greater than 200%" which were ascribed to the lack of a unique solution. Therefore, a more realistic approach

#164367 - $15.00 USD Received 9 Mar 2012; revised 20 Apr 2012; accepted 23 Apr 2012; published 3 May 2012

would involve the use of a noninvasive technique like optical coherence tomography to determine D, and the development of NN models for a range of individual D values.

Prior theoretical studies of layered tissue OP measurement relevant to UV-Vis spectroscopy of mucosal tissue have also shown promising results. Liu and Ramanujam [30] sequentially estimated OPs of superficial and deep layers, using probe designs that enabled depth-selectivity and an inverse MC for the OP determination from reflectance values. They identified percentage deviation (averaged over wavelength range) ranges of −14.7% to 31.4% for $\mu_{a1}$, −12.6% to −5.3 for $\mu_{s1}'$, −12.6% to 6.6 for $\mu_{a2}$, and −18.3 to −1.8% for $\mu_{s2}'$. Error varied significantly with D, but without any apparent trends. The OP ranges of this study were limited to $\mu_a$ = 1-10 $cm^{-1}$ and $\mu_s'$ = 7-30 $cm^{-1}$, with the primary chromophore being nigrosin rather than Hb. Tseng *et al.* [10] developed an algorithm that simultaneously analyzed the spectral and spatial reflectance spectroscopy data based on an iterative fitting approach. For D = 0.3 mm, theoretical estimation error varied from 0.2% to 11%. Although D ranged from 0.1 to 0.6 mm, no data was provided regarding its influence on estimation accuracy. Some limitations to Tseng *et al*'s study include the 8-12 hours required for fitting and the relatively narrow OP range studied ($\mu_{a1}$ = 0.01-7.22 $cm^{-1}$, $\mu_{s1}'$ = 6.25-12.5 $cm^{-1}$, $\mu_{a2}$ = 0.03-18.06 $cm^{-1}$, $\mu_{s2}'$ = 15.41-28.06 $cm^{-1}$), as well as the use of Hb as a superficial layer absorber. In general, the results of these prior studies are comparable to our theoretical results, although it is difficult to anticipate the true level of accuracy that would be achieved by these approaches under experimental conditions.

One of the prime sources of error in the current study results is likely the extremely large parameter space represented by four OP values [$\mu_{a1}$, $\mu_{s1}'$, $\mu_{a2}$, $\mu_{s2}'$]. Using single-layer MC and NN models and the current experimental-analytical approach to estimate OPs of single layer phantoms, we achieved mean prediction errors of 4% for $\mu_a$ and $\mu_s'$ as compared to 14-42% errors for layered phantoms. This result illustrates that OP estimations in layered tissue are subject to greater error than for homogeneous media. The degradation in predictive ability stems in part from the need to determine four OP values based on a limited set of diffuse reflectance values, which increases the likelihood of non-unique solutions—multiple sets of OPs that produce similar reflectance distributions [12]. Another source of error came from the size of OP range. A wider OP range appears to cause larger errors. Additionally, layered tissue introduces problems such as low sensitivity of reflectance to OP changes under certain conditions (e.g., thin superficial layers).

One of the more encouraging results was the finding that the disagreement between true and estimated values in experimental results (Figs. 7 and 8) was, in most cases, smaller than the change in OPs from normal to dysplastic tissue. While the sensitivity to detect dysplasia-induced changes is not evident in all cases (e.g., $\mu_{a1}$), OP estimation error does appear to be significantly smaller than the expected change in OPs between normal and dysplastic tissue in other cases (e.g., $\mu_{s1}'$, $\mu_{a2}'$). The ratio of error to difference is important to allow measurement of variations due to standard biological conditions and tissue inhomogeneity as well as to the evaluation of OP changes that occur during progression from normal to dysplastic tissue as well as to cancer. Furthermore, the ability to reliably discriminate between normal and diseased tissue on the basis of OPs may enable this approach to facilitate the detection of neoplastic changes.

Although the experimental results are encouraging, additional testing and improvements will be needed to achieve a consistently high level of measurement quality. While nonlinear optimization fitting improved the accuracy of predicted OPs, additional methods may be needed to reduce the effect of crosstalk. One method to improve original OP measurement may involve selecting specific phantoms for calibration [31]. However, the drawback of this method was that the OP range of calibration phantoms should be similar to that of the samples.

#164367 - $15.00 USD Received 9 Mar 2012; revised 20 Apr 2012; accepted 23 Apr 2012; published 3 May 2012

## 5. Conclusions

By combining condensed MC modeling, two-stage NN inverse modeling and nonlinear spectral fitting algorithms with a broadband reflectance spectroscopy system, we developed a novel approach for determination of UV-Vis OPs in layered turbid media. We evaluated this system theoretically and experimentally with phantoms simulating normal and dysplastic epithelial tissue in the 350-600 nm range, and found that it had the capability to provide moderately accurate OP results under most conditions. We were able to measure OPs of selected mucosal-tissue-simulating phantoms ($\mu_a$ = 0.01–25 $cm^{-1}$, $\mu_s'$ = 1–50 $cm^{-1}$) in the UV-Vis range with mean absolute errors that ranged from 14 to 42% under a variety of conditions. While additional modifications may improve performance, these results indicate that our approach should be able to provide useful broadband OP measurements of layered biological tissues such as mucosa.

## Appendix A: Disclaimer

The mention of commercial products, their sources, or their use in connection with material reported herein is not to be construed as either an actual or implied endorsement of such products by the Department of Health and Human Services.

#164367 - $15.00 USD Received 9 Mar 2012; revised 20 Apr 2012; accepted 23 Apr 2012; published 3 May 2012